SUPPLEMENTAL INFORMATION

Cytoskeletal mechanisms of axonal contractility

S. P. Mutalik, J. Joseph, P.A. Pullarkat and A. Ghose

List of supplementary figures:

List of supplementary videos:

Supplementary Materials and Methods

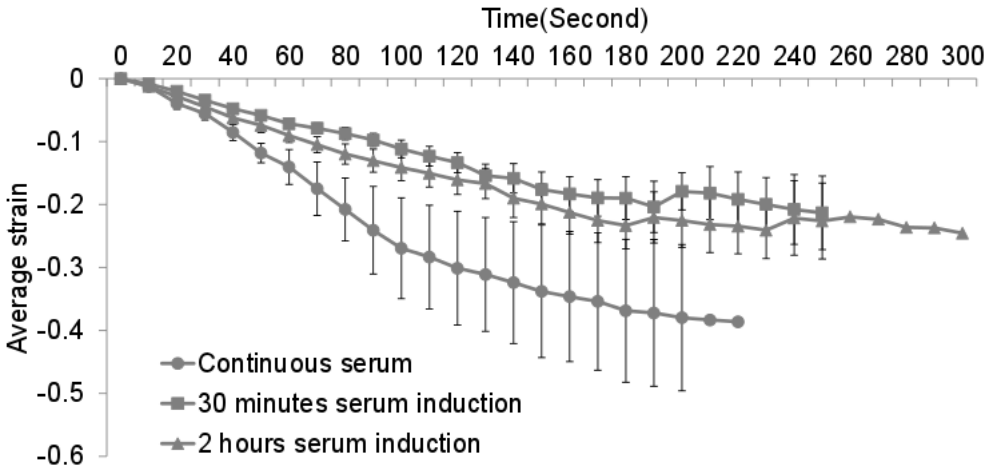

S1. Strain relaxation after de-adhesion in axons grown under different serum conditions. Neurons were cultured for 48 hours with either serum-containing media (continuous serum) or in serum-free media. Neurons growth without serum were supplemented with 10% serum for either 2h or 30 mins prior to de-adhesion. Average strain is plotted for continuous serum (n=7) or serum supplementation for 2 hours (n=7) or for 30 minutes before trypsin de-adhesion (n=14). While the strain rate is slightly larger for neurons grown continuously in serum, the rates for 2 hours and 30 minutes induction were comparable. Short serum induction (2 hours or 30 minutes) resulted in more curved neurons at the time of the experiment compared to those grown in continuous serum.These results prompted us to use the 30 minute serum induction paradigm for all further experiments. Error bars represent standard error of the mean.

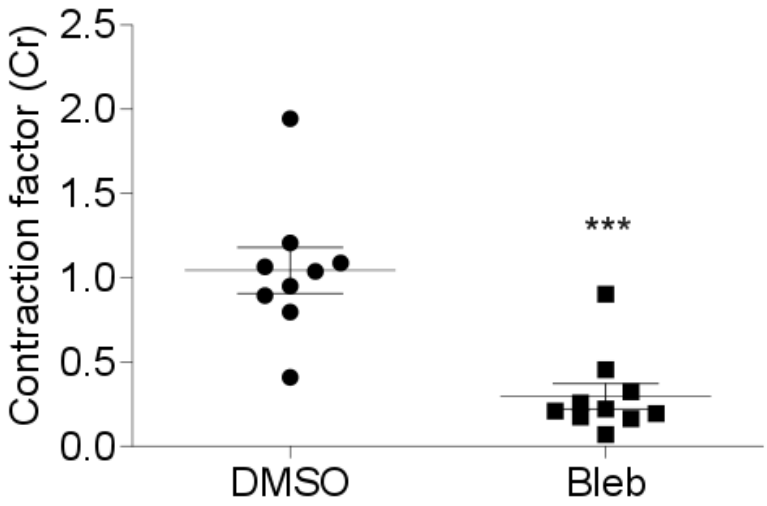

S2. Inhibition of myosin II affects the extent of axonal contraction. The contraction factor is significantly reduced ($p = 0.0001$) upon Blebbistatin (Bleb; 30 μM pretreated for 1 hour prior to trypsin addition; $n = 10$) treatment compared to DMSO control ($n = 9$) treated axons.

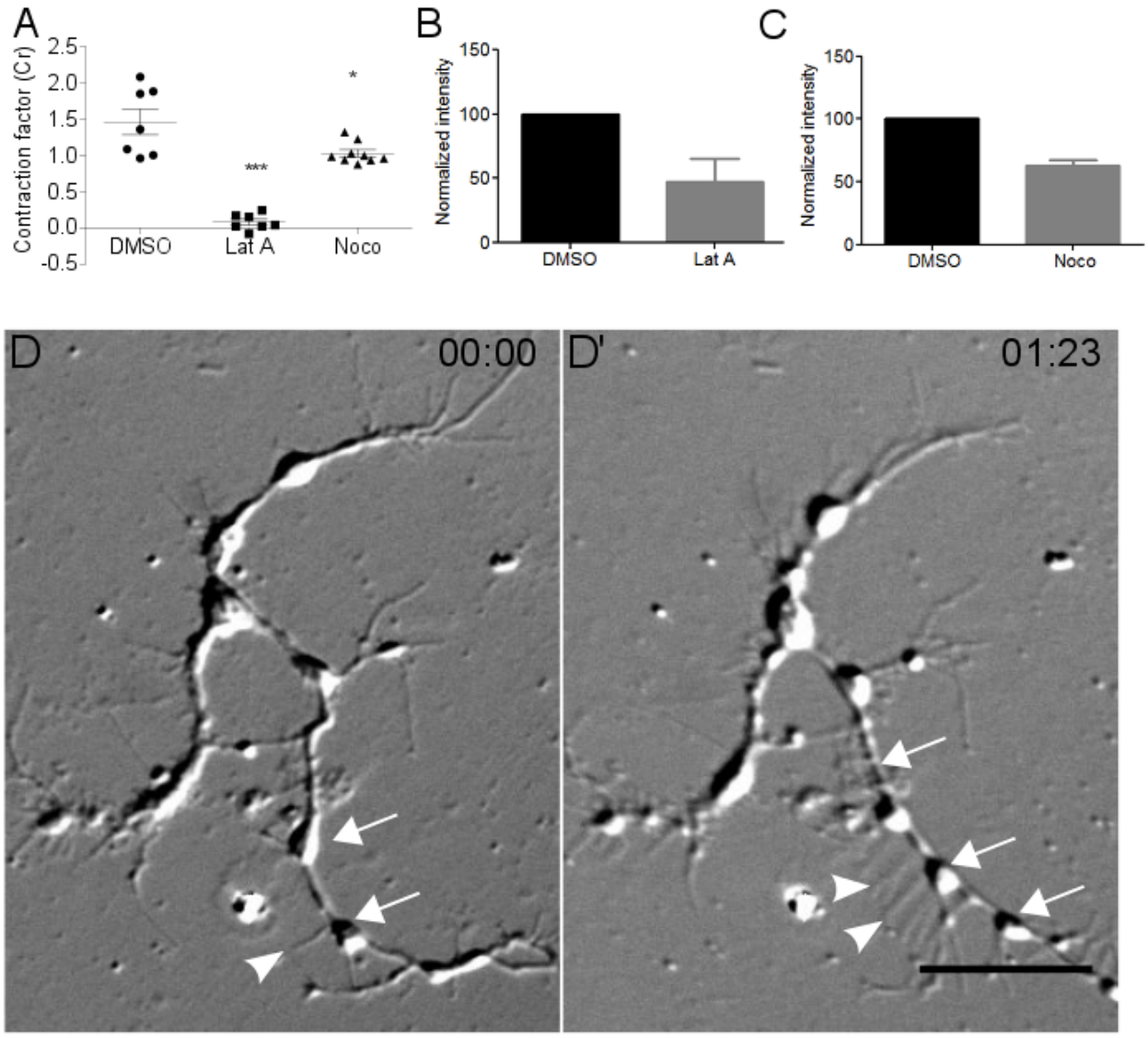

S3. Effect of F-actin and microtubule disruption on axonal contraction, cytoskeleton organisation and axonal morphology. (A) The contraction factor is strongly reduced ($p < 0.0001$) upon Latruculin A (Lat-A; 0.6 µM pretreated for 15 mins prior to trypsin addition; n = 7) treatement compared to DMSO treated axons (n = 7). Nocodazole treatment (Noco; 33 µM pretreated for 15 mins prior to trypsin addition; n = 9) also resulted in a marginal decrease ($p = 0.0204$). Unpaired t-test was used to compare the means. Error bars represent standard error of the mean. (B,C) Efficacy of drugs. (B) Lat A (Lat-A; 0.6 µM pretreated for 15 mins) treated axons show reduced intensity of actin in phalloidin stained neurons. (C). Noco (Noco; 33 µM pretreated for 15 mins) treated axons show reduced intensity of microtubules in microtubules stained neurons. (D) Representative micrograph of axons pretreated with 33 µM Nocodazole for 15 minutes

before trypsin addition at time 0. (D') Micrograph of the same axon after addition of trypsin. Time elapsed is indicated in minutes:seconds. Extensive beading (white arrows) and formation of tethers (white arrowheads) are observed in Nocodazole-treated axons. Scale bar: 15 μm.

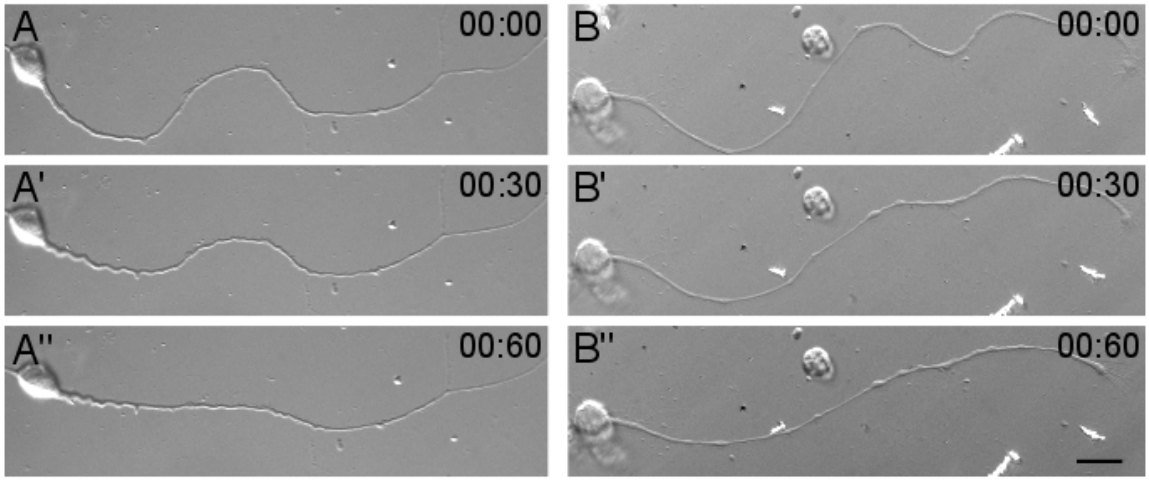
A
00:00
B
00:00
A'
00:30
B'
00:30
A''
00:60
B''
00:60

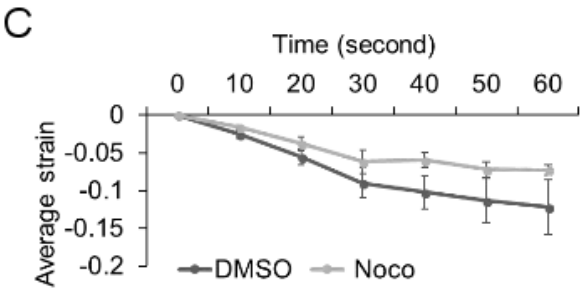
C
Time (second)
0
10
20
30
40
50
60
Average strain
0
-0.05
-0.1
-0.15
-0.2
DMSO
Noco

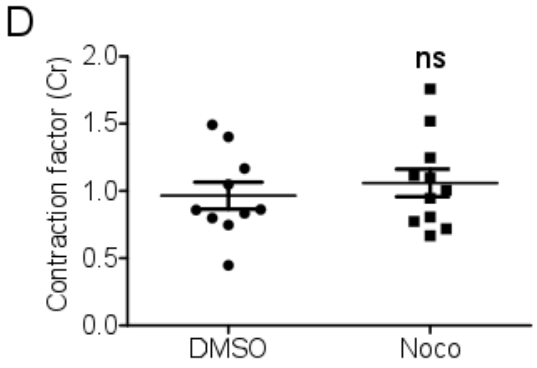
D
Contraction factor (Cr)
2.0
1.5
1.0
0.5
0.0
ns
DMSO
Noco

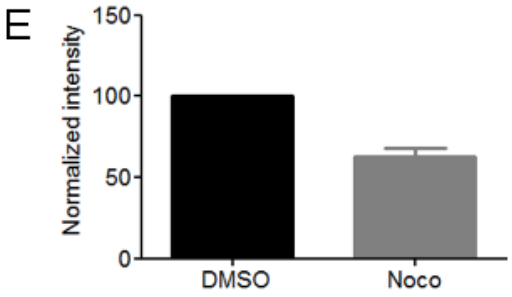
E
Normalized intensity
150
100
50
0
DMSO
Noco

S4. Microtubule depolymerization with the lower concentration of Nocodazole (16 μM) reduces the rate of axonal contraction. (A-A”) and (B-B”) are representative frames from time-lapse imaging of an axon pretreated for 15 mins with DMSO and Nocodazole (16 μM), respectively. Trypsin is added at time 0 for each treatment. Time stamp shows minutes: seconds elapsed. Scale bar: 15 μm. (C) Average strain rate is reduced upon Nocodazole (Noco) treatment (n =11) compared to DMSO-treated controls (n =10). Error bars indicate standard error of the mean. (D). Contraction factor doesn’t change upon Noco (16 μM) treatment. (E) Noco (16 μM pretreated for 15 mins) treated axons show reduced intensity of alpha-tubulin immunofluorescence signal.

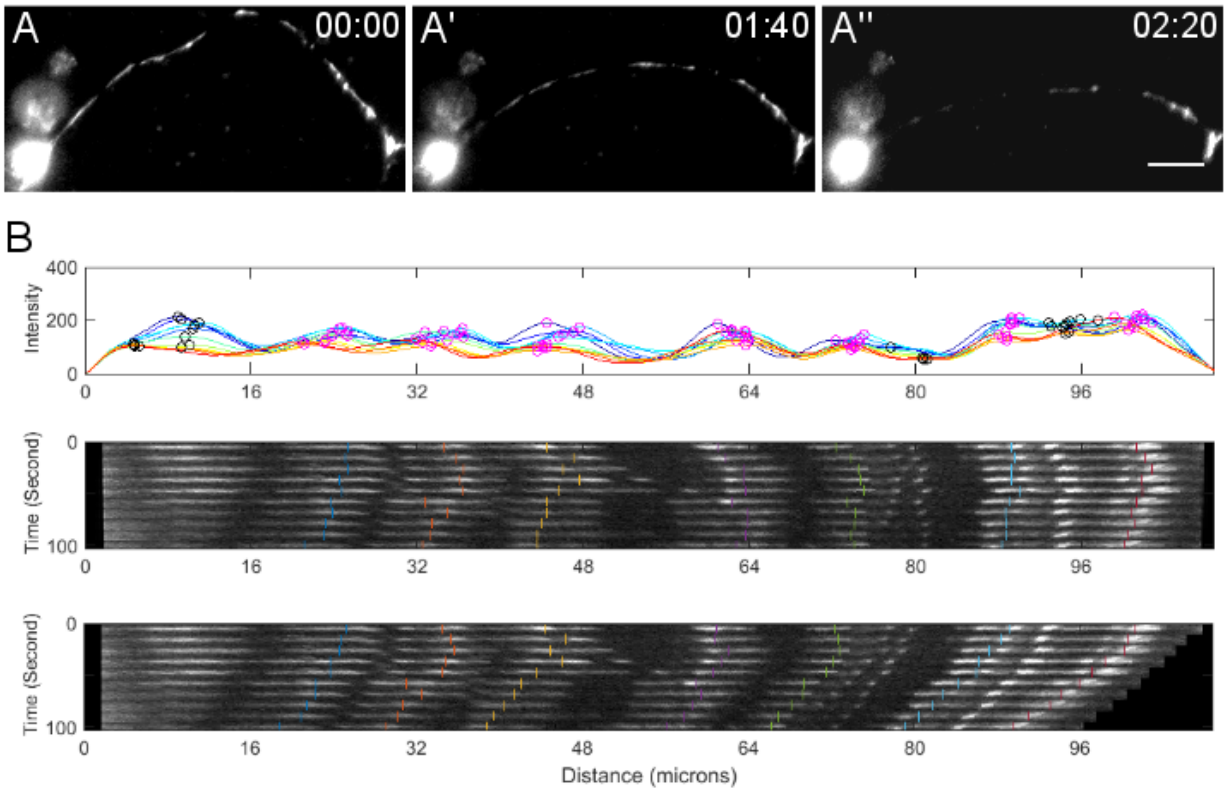

S5. Mitochondria tracking and analysis. (A-A'') Representative time frames of an axon with labeled mitochondria undergoing straightening due to induced de-adhesion. Trypsin was added at time 0. Time elapsed is in minutes:seconds. Scale bar: 15 μm. (B) Intensity-based detection of mitochondrial position along the axon, from the cell body to the distal end (see Materials and Methods for details). The top panel shows the intensity traces for different timepoints (represented in different colors) along the axon. The intensity trace of each timepoint is resampled to have the same length as the first timepoint (longest). The positions of the detected local maxima are indicated by circles. Pink circles indicate maxima selected for analysis while black circles mark positions of mitochondria which were not included for analysis. The middle panel shows a kymograph of the fluorescent mitochondria with the axonal contours at each timepoint stretched to the same length. This procedure serves as a visual aid to reliably identify peaks corresponding to mitochondria that are reliably present across all time points. The bottom panel shows a kymograph in the original scale with the the location of the selected mitochondria (rescaled to the actual scale), which were used to calculate local strain. In this representation, length shortening is seen due to axonal straightening. In both of the kymographs (middle and bottom panels) the origin is fixed at the side of the soma (left side) and each selected mitochondrion marked with a unique color across time.

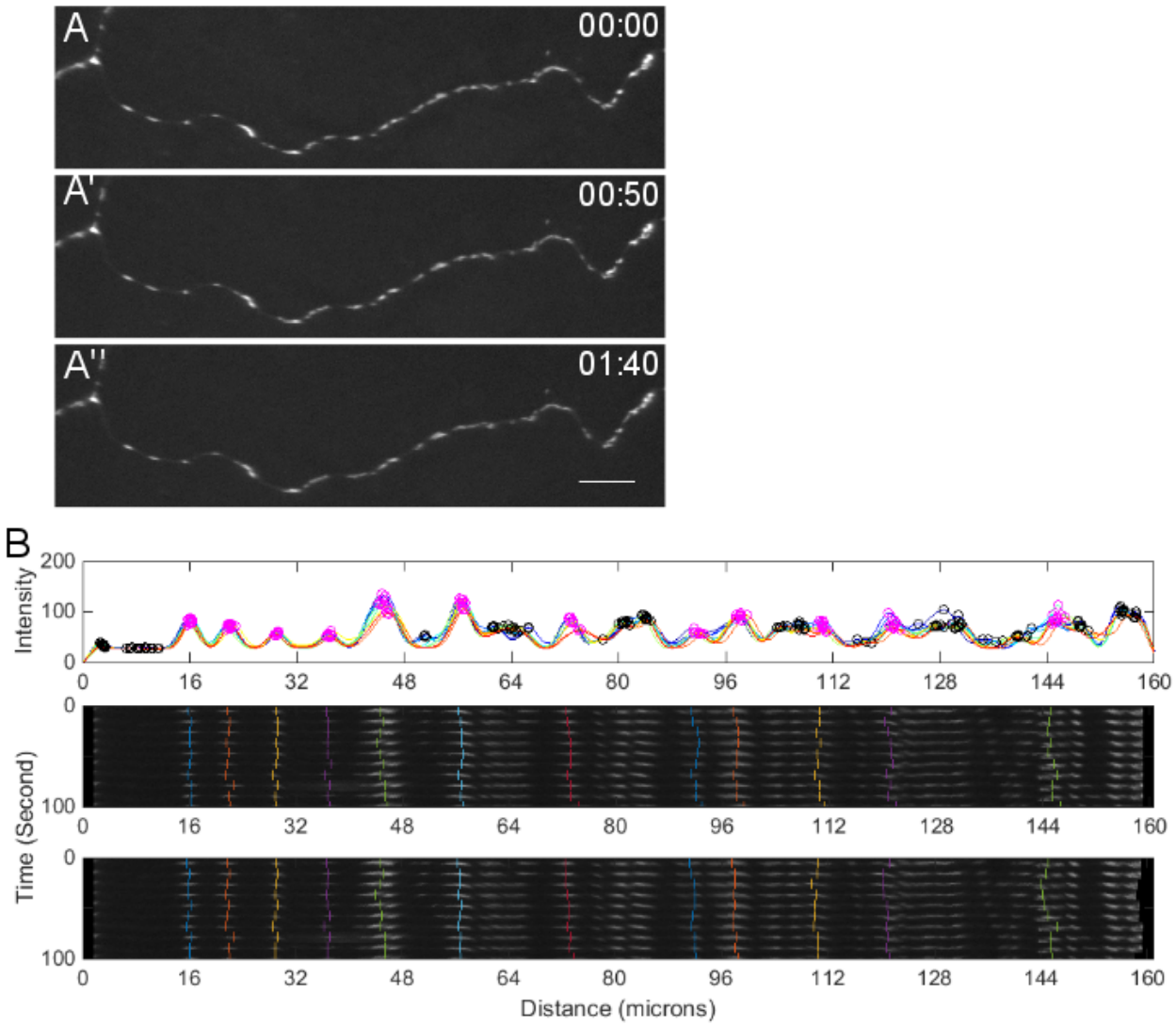

S6. Baseline fluctuations of mitochondria positions in the absence of contraction. (A-A'') An example of baseline mitochondria fluctuations without the trypsin flow. (B) Top panel shows intensity profile of mitochondria for the axon without de-adhesion and straightening. Bottom panel shows kymograph of the fluorescent mitochondria with the axonal contours at each timepoint stretched to the same length. The bottom panel shows a kymograph in the original scale with the location of the selected mitochondria (rescaled to the actual scale). In this representation, no length shortening is observed. In both of the kymographs (middle and bottom panels) the origin is fixed at the side of the soma (left side) and each selected mitochondrion marked with a unique color across time.

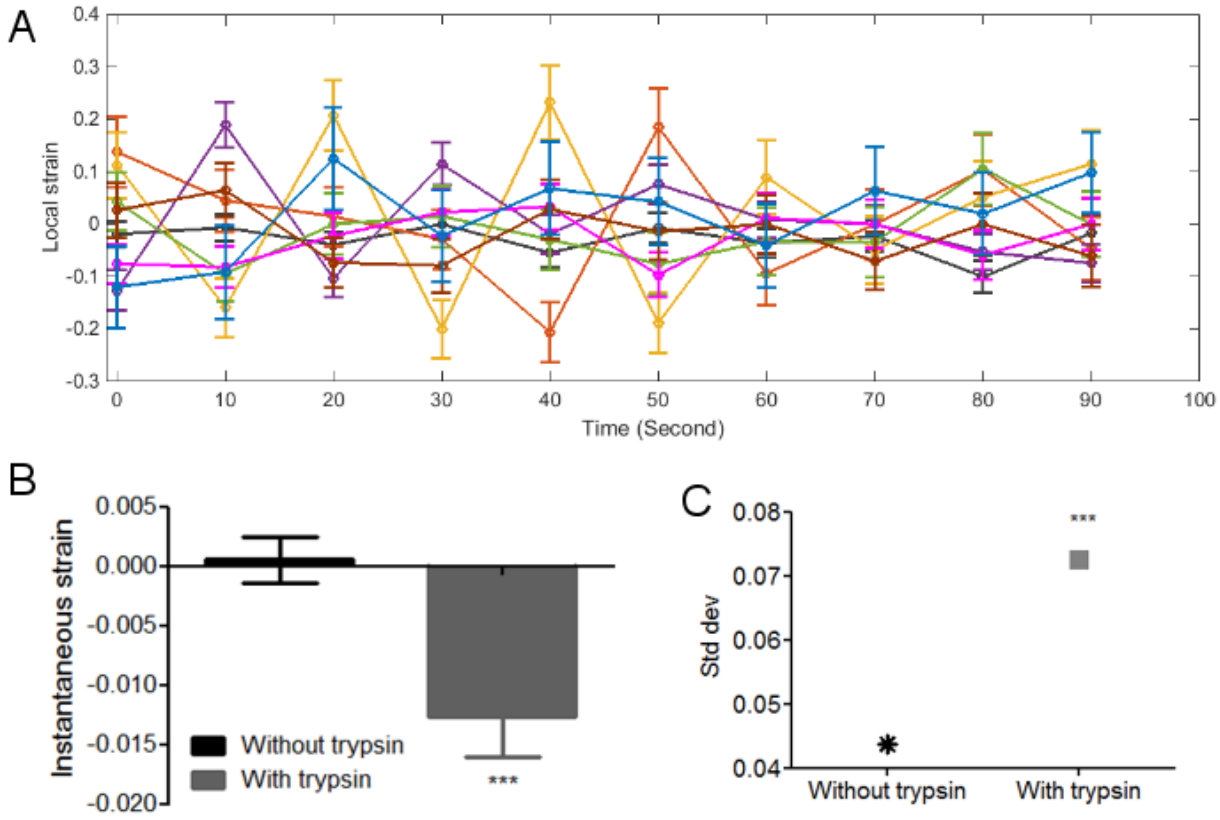

S7. Strain heterogeneity upon axonal contraction. (A) Instantaneous strain ($\Delta L_i(t+\delta t) - \Delta L_i(t)) / \Delta L_i(t)$) between pairs of mitochondria for the same axon shown in Figure 5. Color coding for mitochondrial pairs is the same as in Figure 5. (B) Average instantaneous strain is negative upon trypsin treatment and contraction (p=0.0009). Student t-test with Welch's correction was used to compare means (without trypsin; n=6, with trypsin; n=8) . (C). Comparison of variances reveal that strain heterogeneity increases upon de-adhesion initiated contraction. Comparison performed using the O'Brien's test (p=0.0001.)

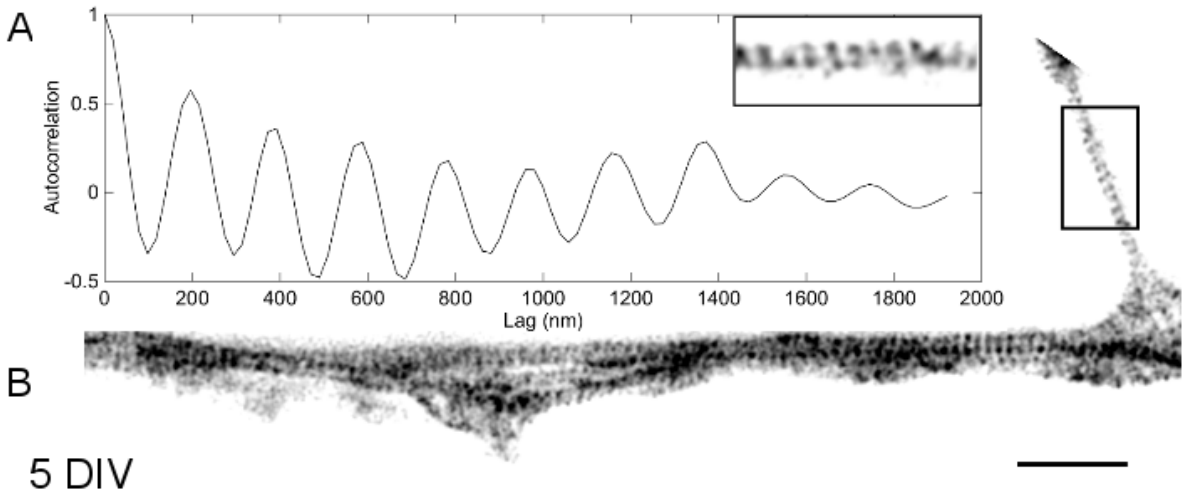
A
Autocorrelation
1
0.5
0
-0.5
0
200
400
600
800
1000
1200
1400
1600
1800
2000
Lag (nm)
B
5 DIV

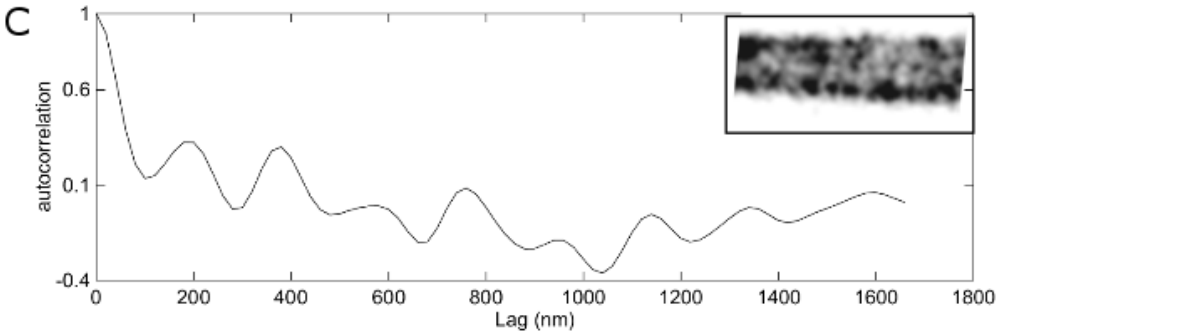
C
autocorrelation
1
0.6
0.1
-0.4
0
200
400
600
800
1000
1200
1400
1600
1800
Lag (nm)


D
2 DIV

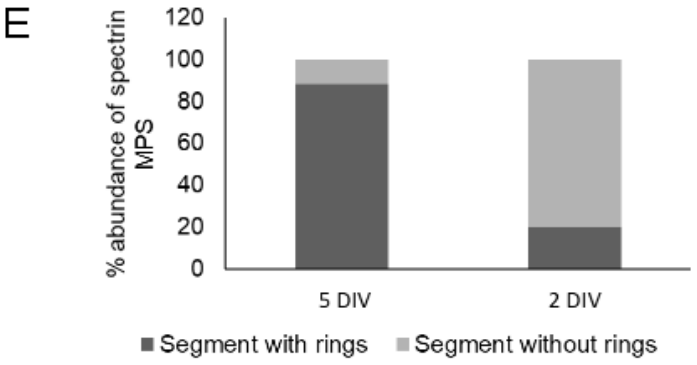
E
% abundance of spectrin MPS
120
100
80
60
40
20
0
5 DIV
2 DIV
Segment with rings
Segment without rings

S8. ßII spectrin organization in chick DRG axons. (A) Autocorrelation graph for the region boxed in B (shown in the inset). (B). Representative STED micrograph of a ßII spectrin labelled axon from a fixed 5 DIV DRG culture showing spectrin MPS. (C). Autocorrelation graph for the region boxed in D (shown in the inset). (D) Representative STED micrograph of a ßII spectrin labelled axon from a fixed 2 DIV DRG culture. At this stage spectrin MPS is not abundant and the autocerration not as robust compared to 5 DIV. (E) Comparison of abundance of ßII spectrin periodic rings between 5 DIV (n=24) and 2 DIV (n=24) neurons. Scale bar: 2 µm.

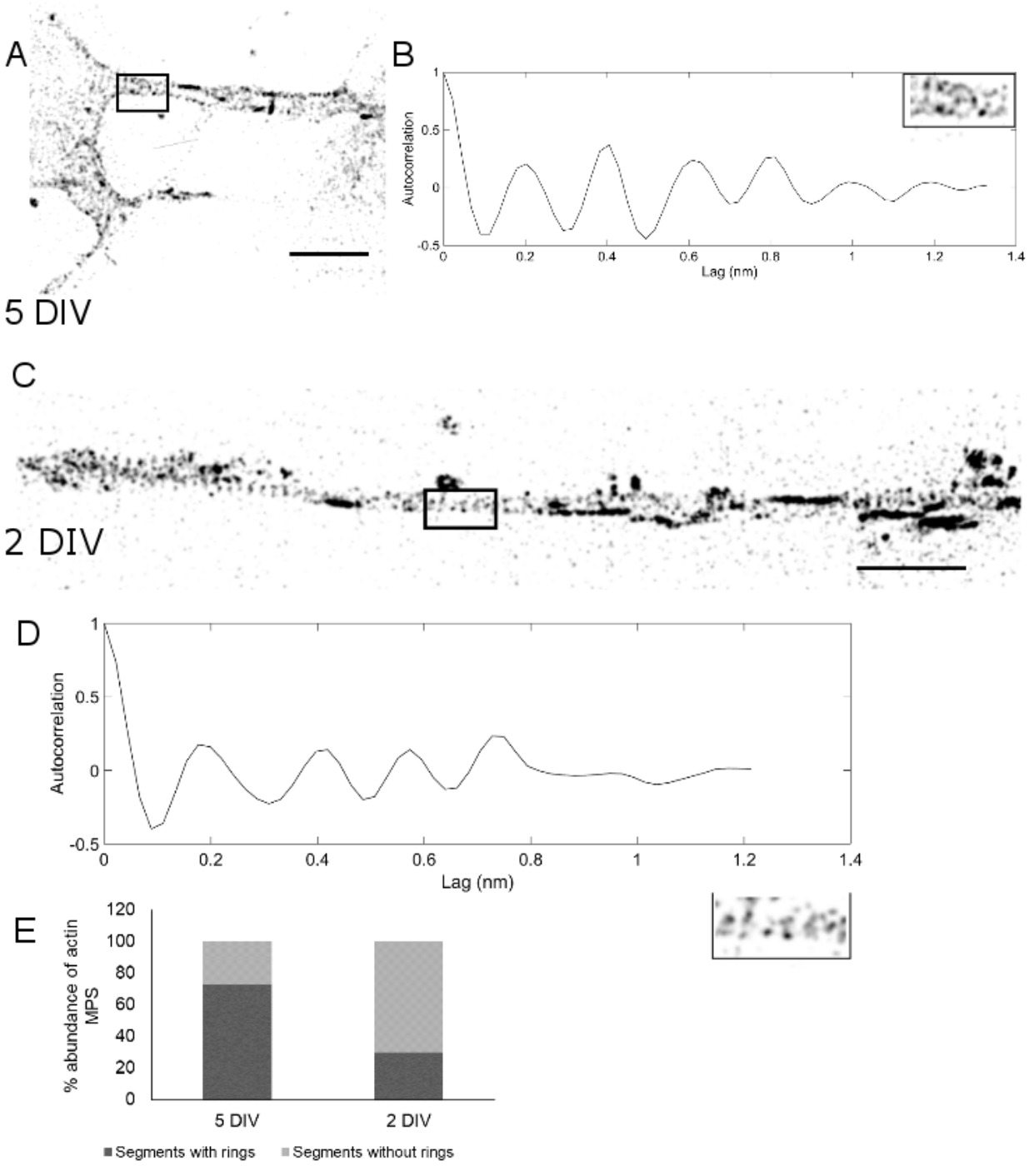
A
B
Autocorrelation
Lag (nm)
5 DIV
C
2 DIV
D
Autocorrelation
Lag (nm)
E
% abundance of actin MPS
5 DIV
2 DIV
Segments with rings
Segments without rings

S9. F-actin organization in chick DRG axons. (A) Representative STED micrograph of a SiR-actin labelled live axon from a 5 DIV DRG culture. (B) Autocorrelation graph for the region boxed in A (shown in the inset). (C) Representative STED micrograph of a SiR-actin labelled live axon from a 2 DIV DRG culture. At this stage F-actin rings are not abundant though F-actin patches and elongated patches are occasionally present. This image has been chosen to show occasional regions that have periodically organized F-actin, though these are not abundant at this stage (D) Autocorrelation graph for the region boxed in D (shown in the inset). (E) Comparison of abundance of actin MPS between 5 DIV (n=34) and 2 DIV (n=47) neurons. Scale bar: 2 μm.

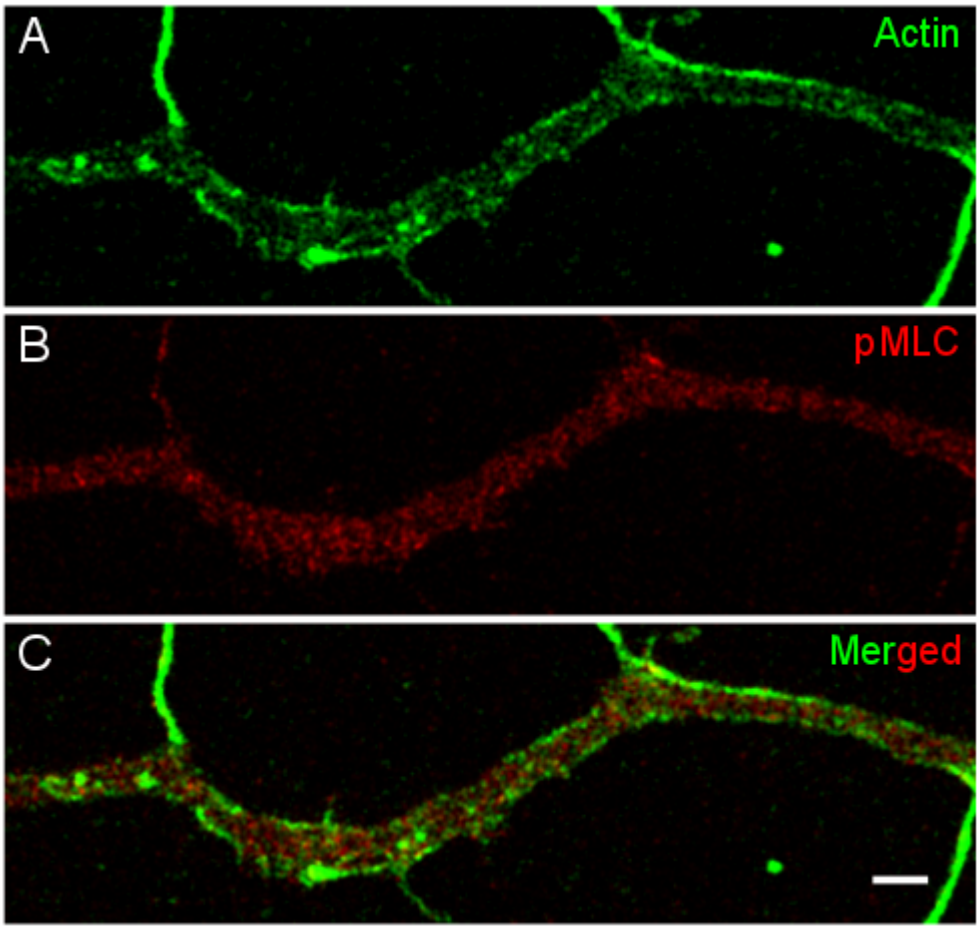

S10. Actomyosin organization in 2 DIV axons. Representative STED micrograph of a 2 DIV DRG axon stained with phalloidin (A) and pMLC (phosphorylated myosin light chain; B). (C) Merged image for the the phalloidin (green) and pMLC (red) signals. Scale bar: 2 μm.

SUPPLEMENTARY MATERIALS AND METHODS

Immunostaining:

5 DIV and 2 DIV cultures were fixed using 3.5% paraformaldehyde and 0.05% glutaraldehyde in PHEM buffer (60 mM PIPES, 25 mM HEPES, 10 mM EGTA, 2 mM Mgcl2.6H2O, pH 6.9) for 10 minutes, followed by 3 washes with the PHEM buffer. For βII spectrin staining experiments, neurons were permeabilized with 0.2% Triton-X (Sigma) for 5 minutes, followed by three washes with PHEM buffer and blocking in 3% BSA (SRL) for 1 hour. Primary antibody was incubated overnight at 4^0C (anti βII spectrin anitibody 1:1500, BD Biosciences). Anti mouse IgG conjugated to Alexa Fluor 568 (Invitrogen) was used as the secondary antibody. For STED imaging, samples were mounted in Mowiol (2.4% Mowiol 4–88 (poly(vinyl alcohol), Sigma) and DABCO (2.5% w/v, 1,4-diazobicyclo[2.2.2]octane, Sigma) mounting medium.

For drug efficacy experiments, 2 DIV cultures were treated with Latrunculin A (0.6 µM for 15 minutes), Nocodazole (16 µM and 33 µM for 15 minutes) or appropriate DMSO controls and then fixed as described earlier. Neurons were permeabilized for 30 minutes using 0.5% Triton-X (Sigma). Permeabilization was followed by three washes in PHEM buffer and blocking in 3% BSA (SRL) for 1 hour. Actin was labelled with Phalloidin conjugated with Alexa Fluor 488 (1:100 for 45 minutes, Invitrogen). Anti alpha-tubulin antibody DM1A (1:3000, Sigma) was incubated overnight at 4^0C to label microtubules. Immunostaining for phosphorylated myosin light chain was carried out using similar procedures using the anti phosphorylated serine 19 myosin light chain 2 antibody (pMLC, 1:100, Cell Signaling Technology). Anti mouse IgG conjugated with Alexa Fluor 568 (1: 1000, Invitrogen) was used as the secondary antibody to label microtubules while anti rabbit IgG coupled with Alexa Fluor 568 (1:1000) was used for pMLC staining.

Staining of live neurons with SiR actin:

For live STED imaging of actin, neurons were labelled with SiR actin (3 uM in the culture medium for 1 hour, Cytoskeleton, Inc.). Washed 3 times with L15 and imaged in the L15 medium containing B27.

Imaging and intensity analysis:

For drug efficacy experiments, both DMSO treated and drug treated neurons were imaged using using a 100x oil objective on an Olympus IX81 system equipped with a Hamamatsu ORCA-R2 CCD camera. Images were recorded using the Xcellence RT (Olympus) software. Exposure was maintained at 50 ms - 100 ms range to avoid saturating conditions. Control and treated samples imaged using the same settings.

Intensity along axons were calculated using the Image J segmented line tool and mean intensities were compared across DMSO control and the drug treatments. For each set, intensity was normalized to control, then averaged over of all sets were compared.

STED imaging and analysis:

STED imaging was carried out using a Leica TCS SP8 STED nanoscope. Fixed Samples mounted in Mowiol-DABCO were imaged using STED white oil objective lens (HC PL APO 100x/1.40 Oil). For βII spectrin imaging, 561 nm excitation and 660 nm depletion lasers were used. For SiR actin experiments, 650 nm excitation laser and the 775 nm depletion laser were used. For the Phalloidin and pMLC staining experiments, excitation was with the 488 nm and 561 nm lines, respectively. 594 nm and 660 nm wavelengths, respectively, were used for depletion. Live experiments using Sir-actin were done at 37^0C. The raw images were deconvolved using the CMLE JM deconvolution algorithm in the Huygens software (ver 17.04, SVI).

Periodicity of MPS (membrane-associated periodic skeleton; SiR Actin and βII spectrin) was evaluated by plotting the intensity trace along a line using Image J. The intensity values along the line were analysed using the autocorrelation (autocorr) function in MATLAB (2014). For evaluation of abundance of MPS, each axon was selected in Image J using the segmented line tool and its length is divided into smaller segments of 1 μm using a macro. Each segment was visually examined for the presence of MPS and used to calculate percentage abundance [% abundance of MPS=(Number of segments showing MPS)/(total number of segments of MPS)*100] .

Graphical representation and statistics:

Strain vs time plots were generated in Microsoft Excel (2016). Contraction factor and intensity data was plotted and compared in GraphPad Prism 5. Autocorrelation graphs were generated in MATLAB (2014). Heterogeneity analysis was done using the JMP software trial version (JMP 13 SW).